A novel correction for biases in forest eddy covariance carbon balance.

Matthew N. Hayek[a], Richard Wehr[b], Marcos Longo[c], Lucy R. Hutyra[d], Kenia Wiedemann[a], J. William Munger[a], Damien Bonal[e], Scott R. Saleska[b], David R. Fitzjarrald[f], Steven C. Wofsy[a]

[a]Faculty of Arts and Sciences, Harvard University, Cambridge, MA, 02138, USA
[b]Department of Ecology and Evolutionary Biology, University of Arizona, Tucson, AZ, 85721, USA
[c] Embrapa Agricultural Informatics, Campinas, SP, Brazil
[d] Department of Earth and Environment, Boston University, Boston, MA, 02215
[e]INRA, UMR EEF Université de Lorraine / INRA, 54280 Champenoux, France
[f]Atmospheric Sciences Research Center, SUNY Albany, Albany, NY, United States.

Corresponding Author:
Matthew N. Hayek
mhayek@fas.harvard.edu
24 Oxford St.
Cambridge, MA 02143

Keywords:
Carbon dioxide; Amazon; Eddy covariance; Forest carbon flux; Respiration; Friction velocity

Abstract

Systematic biases in eddy covariance measurements of net ecosystem-atmosphere carbon dioxide exchange (NEE) are ubiquitous in forests when turbulence is low at night. We propose an alternative to the conventional bias correction, the friction velocity (u_*) filter, by hypothesizing that these biases have two separate, concurrent causes: (1) a subcanopy CO_2 storage pool that eludes typical storage measurements, creating a turbulence-dependent bias, and (2) advective divergence loss of CO_2, creating a turbulence-independent bias. We correct for (1) using a simple parametric model of missing storage (MS). Prior experiments have inferred (2) directly from atmospheric measurements (DRAINO). For sites at which DRAINO experiments have not been performed or are infeasible, we estimate (2) empirically using a PAR-extrapolated advective respiration loss (PEARL) approach. We compare u_* filter estimates of advection and NEE to MS-PEARL estimates at one temperate forest and two tropical forest sites.

We find that for tropical forests, u_* filters can produce a range of extreme NEE estimates, from long-term forest carbon emission to sequestration, that diverge from independent assessments and are not physically sustainable. Our MS model eliminates the dependence of nighttime NEE on u_*, consistent with findings from DRAINO studies that nighttime advective losses of CO_2 are often not dependent on the strength of turbulence. Our PEARL estimates of mean advective loss agree with available DRAINO measurements. The MS-PEARL correction to long-term NEE produces better agreement with forest inventories at all three sites. Moreover, the correction retains all nighttime eddy covariance data and is therefore more widely applicable than the u_* filter approach, which rejects substantial nighttime data—up to 93% at one of the tropical sites. The full MS-PEARL NEE correction is therefore an equally defensible and more practical alternative to the u_* filter, but leads to different conclusions about the resulting carbon balance. Our results therefore highlight the need to investigate which approach's underlying hypotheses are more physically realistic.

1. Introduction

The terrestrial CO_2 sink, which mitigates approximately one quarter of anthropogenic emissions, is due to an imbalance between photosynthesis, termed gross ecosystem productivity (GEP), and ecosystem respiration (R). Globally, the net ecosystem-atmosphere exchange of CO_2 (NEE) is less than 1% of the two gross fluxes (IPCC, 2013), with global forests representing the majority of this quantity. Much of our process-based knowledge of forest NEE is derived from eddy covariance carbon dioxide flux measurements. However, eddy covariance estimates of NEE during the nighttime (nocturnal carbon efflux or NCE)—which represent R because photosynthesis is inactive at night—are prone to underestimation in the form of a selective

systematic error (Montcrieff et al., 1996), causing an erroneous shift in the net balance towards uptake (Miller et al., 2004). Such biases in forest eddy covariance NCE therefore accumulate in the long-term ecosystem carbon balance.

The predominant explanation for the systematic low bias in NCE is that mean advective flows remove some CO_2 from the subcanopy airspace (Lee, 1998; Sun et al., 1998, Aubinet et al., 2003). This advective divergence loss can be caused by radiative cooling resulting in negative buoyancy, which can move cool CO_2-rich air down slight slopes and into the valleys (Grace et al., 1996) below eddy covariance measurement towers, which are typically placed on plateaus. These mean divergent flows violate the assumption of horizontal heterogeneity upon which the measurements rely.

Based on the assumption that calm, low-turbulence conditions facilitate the advective loss, the now ubiquitous approach to correcting NCE has been to discard nighttime eddy flux measurements when turbulence is low (Wofsy et al., 1993; Goulden et al., 1996; Gu et al., 2005; Reichstein et al., 2005; Papale et al., 2006; Barr et al., 2013). Typically, turbulence is quantified by the friction velocity (u_*) and measurements are discarded when u_* falls below a threshold (u_*^{Th}) below which NCE is observed to decline with u_* and above which NCE is independent of u_*. This method is referred to as the u_* filter approach.

A number of findings, however, cast doubt on the assumption that only calm, low-turbulence conditions facilitate advective divergence loss. Advective losses have been associated with negative buoyancy from thermal gradients, present even when the canopy air is turbulently mixed (Staebler and Fitzjarrald, 2005). Explicit measurements of subcanopy airflow indicate that horizontal advective divergence still occurs when u_* is much higher than the typically applied thresholds (Staebler and Fitzjarrald, 2004; Tóta et al., 2008). Furthermore, such subcanopy

measurements also demonstrate that these horizontal advective fluxes do not account for the NEE correlations with u_*, and sometimes even exacerbate them (Aubinet et al., 2010). An alternative explanation for u_* -dependent biases in NCE is needed.

We propose an alternative set of hypotheses to explain the concurrent phenomena of the apparent u_*-dependence of NCE and the selective systematic error in NEE that leads to underestimation of the long-term carbon budget. The hypotheses are as follows. (1) Hidden CO_2 storage pools below the canopy are underestimated or unobserved by classical concentration profile measurements. The flux from the filling and emptying of these pools is dependent on u_*, and therefore accounts for turbulent-dependent biases, but cannot account for the long-term selective systematic NEE bias towards uptake. (2) Advective loss is independent of u_* but persistently occurs at night and is near zero during the day, and therefore accounts for the long-term selective systematic NEE bias towards uptake. (3) In order to estimate advective loss without explicit measurements of the phenomenon, we further hypothesize that at sunset, both nocturnal advection and photosynthesis are near zero, so eddy flux observations at this time, corrected for storage in both measured and unmeasured pools, are representative of the true *R*. The difference between *R* at sunset and *R* during the rest of the night therefore provides an estimate of advective loss.

Because both our hypotheses and those of the traditional u_* filter are speculative, we intend to highlight that our novel approach results in eddy flux-derived carbon fluxes that are closer to independent assessments of both advective loss and aboveground biomass changes. First, we highlight the problem by demonstrating the traditional technique of correcting NCE biases using a consistent u_* filter method across three sites (two tropical and one temperate forest). Next, we correct for a turbulence-dependent bias in NCE by modeling hypothesis (1)

104 using a simple linear box model to compensate for effects of unmeasured CO_2 storage pools,
105 which are filled or flushed depending on turbulence, but do not add or remove CO_2 from the
106 system on daily or longer timescales. We then add the mean advective loss of hypothesis (2)
107 using prior measurements of subcanopy advection and CO_2 gradients at two of our three sites
108 (Staebler and Fitzjarrald, 2004; Tóta et al., 2008). We also model the advective loss using
109 hypothesis (3), intended for sites lacking measurements of subcanopy flow, and validate the
110 model against the aforementioned measurements. Our approach does not discard any data and
111 consists only of two simple, first-order data corrections, added to observations of forest NEE in
112 sequence, that we hope will ultimately allow for accurate estimates of whole-ecosystem net CO_2
113 fluxes.
114
115 **2. Methods**
116 2.1 Measurements of carbon dioxide and aboveground woody carbon fluxes.
117 We compared eddy flux measurements of NEE to censuses of aboveground woody
118 increment (AGWI) at three sites: (1) the Tapajós National Forest (TNF) km67 in Pará, Brazil
119 (Rice et al, 2004; Hutyra et al., 2007; Pyle et al., 2008), (2) Guyaflux in Paracou, French Guiana
120 (Bonal et al., 2008; Rowland et al., 2014), and (3) the Harvard Forest in Petersham,
121 Massachusetts, USA (Wofsy et al., 1993; Urbanski et al., 2007). Eddy flux records covered: (1)
122 January 2002-January 2006 and August 2008-December 2011 at TNF km67, (2) 2005-2014 at
123 Guyaflux, and (3) 1992-2013 at the Harvard Forest.
124 The NEE data were quality-controlled half-hourly or hourly values, calculated as the sum
125 of the eddy flux and the measured storage flux (i.e. the rate of storage of CO_2 in air spaces in the
126 subcanopy and canopy, below the eddy flux sensor height). Half-hourly values were averaged to

127 an hourly timestep in order to have uniform minimum time steps across all three sites. The
128 hourly NEE observations are herein referred to as NEE_{obs}, to distinguish them from subsequent
129 bias-corrected values. The nighttime subset of hourly NEE_{obs} is referred to as NCE_{obs}.
130 To calculate yearly and longer-timescale sums of both NEE_{obs} and bias-corrected NEE,
131 hourly data were gap-filled using parametric relationships of daytime NEE with
132 photosynthetically active radiation (PAR) and air temperature (Falge et al., 2001; Dunn et al.,
133 2007; Urbanksi et al., 2007). Gap-filling was performed with independent parameters for the
134 following seasons: wet and dry seasons at TNF km67 and Guyaflux, with each year treated
135 independently, and 8 seasons at the Harvard Forest, with each decade treated independently.
136 Gap-filled data were only used to produce long-term total and annual mean NEE; non-gap-filled
137 NEE_{obs} were used for the rest of the analysis. We estimated 95% confidence intervals due to
138 random measurement errors for annual and total mean NEE by bootstrapping, i.e. randomly
139 resampling (with replacement) hourly NEE_{obs} from similar seasons, years, and PAR and
140 temperature conditions.
141 Biometry censuses covered (1) 1999, 2001, 2005, and 2008-2011 for TNF km67, once
142 per year in the early dry season, (2) 2004, 2006, 2008, and 2013 for Guyaflux, once per year in
143 March, and (3) 1993 and 1998-2013 for the Harvard Forest, once in July 1993 and four times per
144 year in 1998-2013. At all sites, AGWI was calculated as the annual increase in aboveground
145 woody biomass (AGWB) in trees with diameter at breast height (DBH) $\geq$ 10 cm, plus additions
146 from recruitment minus losses from mortality. AGWI 95% confidence intervals were produced
147 by bootstrapping, i.e. randomly resampling yearly subplot-based subtotal AGWB with
148 replacement in the case of TNF km67 and Guyaflux, and randomly resampling yearly total
149 AGWI with replacement in the case of the Harvard Forest.

150

151 2.2 Change-point detection for a conventional u_* filter approach

152 We applied a conventional u_* filter to NCE_{obs} (nighttime-only NEE_{obs}) and quantified the
153 resulting net carbon balance in annual and long-term sums of u_* filtered NEE_{obs}. We used the
154 change-point detection method (CPD) for selecting u_*^{Th} due to its insensitivity to noise in the
155 NCE vs. u_* relationship and its prior validation at a suite of 38 North American forest eddy
156 covariance sites (Barr et al., 2013). The CPD method consists of two steps: (1) binning the
157 NCE_{obs} and u_* data into n_B equally sized u_* classes and (2) modeling the response of binned
158 NCE_{obs} vs. u_* as two intersecting linear regressions, with their intersection representing the
159 threshold, u_*^{Th}, below which data are discarded.

160 For each site, we modified step (1) from the original CPD method by binning NCE_{obs} and
161 u_* for all years, instead of each individual year. Results were robust to a large range of values for
162 n_B, but we selected a value of $n_B = 500$ for every site to allow our binning to include substantial
163 information in the long tail of the u_* distribution. For step (2), Barr et al. (2013) included two
164 versions of the change-point regression approach in their analysis: one for which the second
165 regression has a fitted slope (increasing or decreasing high-u_* response), and another for which
166 the slope is simply zero (no high u_* response). For parsimony, we used the second approach for
167 all sites. Their CPD model is:

168
$$NEE_{obs,i} = \begin{cases} a_0 + a_1 u_{*_i} + \varepsilon, & 1 \le i \le c \\ a_0 + a_1 u_{*_c} + \varepsilon, & c \le i \le n \end{cases} \quad (1)$$

169 where i is a discreet index of the independent variable u_* to ensure that the intersection between
170 the two linear regressions lies within the interval between i=1 and i=n. The fitted linear
171 regression parameters a_1 and a_0 are calculated for each value of u_* change points u_{*c} from c=*2* to
172 c=*n-1*. The most probable value of u_{*c} is the one that minimizes the sum of squared errors for its

respective double regression. We set this value of u_{*c} to be our final u_*^{Th}. Errors in u_*^{Th} are reported as 95% confidence intervals, generated by bootstrapping: we randomly sampled pairwise NCE_{obs} -u_* observations with replacement and regenerated regressions for 501 simulations, recalculating u_*^{Th} for each simulation. Using the CPD technique for u_*^{Th} detection allowed us to apply a consistent, conventional u_* filter approach to NCE_{obs} from disparate forest sites.

The CPD is not the only u_* filter selection algorithm; the debate between which algorithm is most prudent is still active (Barr et al., 2013; Galvagno et al., 2017). To present the full ranges long-term carbon balance with respect to various u_* filters, we used a spectrum of u_* thresholds at each site to recalculate annual and long-term total NEE_{obs}: u_*^{Th} = 0, 0.1, 0.2, 0.3, 0.4, the commonly used literature u_*^{Th} value, and our CPD u_*^{Th} calculation from Eq. 1. In the case that our CPD u_*^{Th} result agreed with the literature u_*^{Th} value within 95% confidence intervals, we used the literature u_*^{Th} value to produce results consistent with previous studies. Using a wide range of u_*^{Th} values allowed us to demonstrate how using *any* type of u_* filter, not merely the CPD, compares with our alternative correction, which is described in the following sections.

2.3 An alternative correction: MS-PEARL

Our full correction takes the form of two addends to standard measurements of forest NEE_{obs}:

$$NEE = NEE_{obs} + \frac{dC_2(u_*,t)}{dt} + A(t); \qquad \mathrm{NEE}_{\mathrm{obs}} = fCO_2 + \frac{dC_1}{dt} \tag{2}$$

where fCO_2 is the measured eddy covariance turbulent flux and dC_1/dt is the measured canopy storage flux, i.e. the time derivative of column weighted average of CO_2 concentration measurements, denoted here as C_1. We add two corrective modeled terms to address biases in

196 NEE_{obs}: dC_2/dt is the unmeasured "missing storage" (MS) flux not captured by measurements of
197 dC_1/dt, and $A(t)$ is the mean advective divergence loss.

198 Our MS flux model is described in Section 2.3.1. The MS term is intended to correct for
199 the turbulent-dependent biases in NEE_{obs}, which includes the classical storage column
200 measurement. Our MS flux model is agnostic to where the missing storage pool is located. We
201 offer three hypotheses for the location of this pool, which are not mutually exclusive: (1) a
202 horizontally disparate location, outside of the CO_2 storage column measurement footprint, but
203 within the relatively large footprint of the above-canopy eddy flux sensor, (2) the airspace above
204 the leaf litter layer but below the lowest CO_2 profile measurement inlet (typically > 0.5-1.0 m
205 above the ground), or (3) the soil pore and leaf litter airspace. Regarding the first hypothesis, we
206 note that flux towers are necessarily located in canopy gaps, and so CO_2 storage in dense
207 canopies may be greater than estimated from measurements on a tower. Identifying the
208 location(s) of the MS pool, however, is outside of the scope of this study; we intend for our
209 hypotheses to serve as an outline for future investigations.

210 Our modeled advective loss estimate *A* is described in Section 2.3.2. We modeled
211 advective loss as turbulence-independent, intending to correct the selective systematic bias that
212 affects long-term NEE (Moncrieff et al., 1996), which likely results from nighttime drainage
213 flows. We also present a summary of prior measurements of advective loss at two of our study
214 sites in Section 2.3.2. Studies suggest that advective loss is primarily related to atmospheric
215 buoyancy (Staebler and Fitzjarrald 2004; van Gorsel et al., 2007; Tóta et al., 2008), not boundary
216 layer turbulence. However instead of modeling the quantitative relationship between potential
217 temperature and advection, we simply utilize the ensemble mean *A* across multiple years for
218 nighttime hours, and assume it is absent at daytime.

2.3.1. Correcting for missing storage (MS)

We developed a simple parametric box model of the unobserved MS flux, dC_2/dt. The flux is positive, negative, or zero depending on the turbulent conditions in that hour and on the accumulated concentration in the previous hour:

$$\frac{dC_2(t_i)}{dt} = \begin{cases} R_2 - \alpha u_*(t_i) & if \quad \frac{C_2(t_{i-1})}{t_i - t_{i-1}} + R_2 > \alpha u_*(t_i) \\ \frac{C_2(t_{i-1})}{t_i - t_{i-1}} & if \quad \frac{C_2(t_{i-1})}{t_i - t_{i-1}} + R_2 \le \alpha u_*(t_i) \end{cases} \quad (3)$$

C_2 represents the hourly CO_2 concentration enhancement above C_1; it is a height-integrated concentration quantity in units of μmol m^{-2}. C_2 is time-integrated across one hourly timestep (t_i-t_{i-1}, expressed in seconds to keep units consistent) once the MS flux into or out of the pool is calculated. By definition, C_2 cannot go below 0, a condition which represents full mixing with the C_1 pool. The two free parameters, R_2 and α, are time-invariant. R_2 is the amount of total ecosystem respiration flux that does not immediately end up in observations of C_1 or fCO_2 in that hour, because it accumulates in the unmeasured storage pool. α is the mixing concentration in units of μmol m^{-3} that, when multiplied by u_*, produces the flushing rate of the unmeasured storage pool. As noted earlier, a precise physical interpretation depends on which hypothesis regarding the location of the MS pool is correct, a question that is outside the scope of this study.

Our MS model parameters, R_2 and α, were fit as follows: for each site, all combinations of the two parameters, rasterized over a range of values, were tested. R_2 and α ranged between 0-6 μmol $m^{-2}s^{-1}$ and 0-40 μmol m^{-3}, respectively, at discrete intervals of 0.1 μmol $m^{-2}s^{-1}$ and 1 μmol m^{-3}, respectively. For every parameter combination in these ranges, the MS model (Eq. 3)

239 was run from an initial value of $C_2(t_0)$=0 in a time-forward manner across the entire eddy flux
240 time series. The cost function was then calculated for the nighttime subset of values. Our cost
241 function was based on the hypothesis that the u_* dependency in the nighttime flux (NCE_{obs}) is
242 solely due to MS flux, not advection or any biological process. Because MS-corrected NCE_{obs}
243 should have minimal u_* dependence at night, our optimization takes the form of minimizing the
244 root mean squared deviation of residual MS-corrected NCE_{obs} around the sample mean value:

245 $$\min \ (RMSD(NCE_{obs} + \frac{dC_2}{dt} - \overline{NCE_{obs} + \frac{dC_2}{dt}})) \quad (4)$$

246 The optimization was intended to find which parameter values resulted in the "flattest"
247 NCE_{obs}+MS vs. u_* relationship, in hopes that the functional form of Eq. 3 could result in a
248 substantial flattening and not a minor one. The combination of parameter values within the raster
249 grid that minimized the cost function for each site were thus taken as the final MS model
250 parameter values, and the MS model was applied to the full NEE_{obs} time series.
251
252 2.3.2. Correcting for advective loss (DRAINO and PEARL)
253 We assume advection is simply constant and positive during the night and zero during the
254 day:

255 $$A(t) = \begin{cases} A_{night}, & night \\ 0, & day \end{cases} \quad (5)$$

256 In actuality, advection is likely dependent upon thermal buoyancy (Staebler and Fitzjarrald,
257 2004), but this relationship was not included due to lack of constraint.
258 At the Harvard Forest and TNF km67 sites, an array of subcanopy measurements of wind
259 speed and CO_2 were deployed in previous studies to estimate the horizontal and vertical
260 advective divergence of CO_2 from the subcanopy airspace (Staebler and Fitzjarrald, 2004; Tóta

et al. 2008). These experiments were dubbed the DRAINO experiments. At both DRAINO sites, exploratory observation campaigns were conducted before primary measurements to determine an optimal sensor network configuration and to characterize the dominant subcanopy flow characteristics. Points of measurement in the subcanopy airspace were made on the corners and edges of a square control area surrounding the tower. Quantifying the spatial scales of advection and CO_2 concentration gradients, as well as the effect size of drag from subcanopy stem density, allowed for the determination of optimal horizontal spacing and orientation of sensors as well as their height, necessary for counteracting the expected small signal-to-noise ratio. Nocturnal flows were also related to physical forcing characteristics below the subcanopy to ensure that they were systematic. The DRAINO measurement campaigns at both sites were able to quantify the transport of CO_2 out of the control volume by identifying the horizontal advective divergence loss process. Both studies reported mean and standard errors for their A_{night} estimates. We used the mean nighttime advection for A_{night} from the multi-year DRAINO campaigns at both sites (growing season only for the Harvard Forest). We call the full NEE correction (Eq. 2) using the DRAINO-derived estimate for A_{night} the MS-DRAINO correction.

Subcanopy measurements of a control volume of airspace beneath eddy covariance towers such as those in the DRAINO campaigns are labor-intensive and costly. Therefore, we devised a method for estimating the advective loss, which we call the PAR-extrapolated advective respiration loss (PEARL). This technique exploits the facts that (1) there is a time delay between nightfall and the onset of thermal gradients that stably stratify the subcanopy airspace and advect CO_2 away from the flux apparatus (van Gorsel et al., 2007) and (2) after correcting for the missing storage flux, NCE_{obs}+MS in the first hour tends to be higher than the rest of the night.

Our PEARL approach for deriving A_{night} from NEE_{obs}+MS builds on that devised by Van Gorsel et. al (2008), who found that the first few hours of the night had more positive CO_2 fluxes. They concluded that this early night "bump" was reflective of the true respiration *R* because the atmosphere remained thermally buoyant and advective loss was insignificant. Our approach builds on theirs with two important additions: (1) we first corrected NEE_{obs} by MS, and found that the bump was present or more prominent after the correction (2) we did not make any assumptions about the precise length of time between sunset and the onset of nocturnal advection (e.g. that it was exactly one hour, the time resolution of our flux measurements, or multiple hours). Instead of identifying the early night bump in time space, we opted for PAR space, taking the limit of evening NEE_{obs}+MS to zero PAR as an approximation of the true *R* absent any advective loss:

$$R = \lim_{\substack{PAR \to 0 \\ T \to T_{night}}} \left(NEE_{obs} + \frac{dC_2}{dt} = a_1 + a_2 T + \frac{a_3 \cdot PAR}{a_4 + PAR} \right) \quad (6)$$

where NEE_{obs} is the observed NEE, *T* is air temperature, dC_2/dt is the MS flux, modeled in Section 2.3.1, and a_2 is the temperature sensitivity parameter separately fit to the nighttime data. We fit the curve using nonlinear least squares regression for NEE_{obs}+MS past noon and a lower PAR threshold of PAR > 0 $\mu mol \cdot m^{-2} \cdot s^{-1}$ to utilize evening values as close as possible to sundown. We used an upper PAR threshold of PAR < 1000 $\mu mol \cdot m^{-2} \cdot s^{-1}$ so that the regression fit was insensitive to the functional form of the high-PAR curvature—hyperbolic, logarithmic, or quadratic—all of which we tested for TNF km67 and include in the discussion of our results. At the tropical sites, we assume $a_2 = 0$ because temperature variability is too small to allow for detection of significant hourly sensitivity (Hutyra et al., 2007).

After fitting the evening PAR curve, the nighttime R equals $a_1+a_2 \cdot \text{mean}(T_{night})$, where T_{night} is the nighttime temperature. Overbars denote long-term averages. Lastly, subtracting the mean MS-corrected NCE_{obs} from the evening-extrapolated estimate for R provides the PEARL estimate for nighttime advection A_{night}:

$$a_1 + a_2 \overline{T_{night}} - \overline{(NCE_{obs} + \frac{dC_2}{dt})} = A_{night} \quad (7)$$

We added the MS and PEARL corrections to NEE_{obs} and reapplied gap filling to the entire time series at the tropical sites, km67 and Guyaflux, and to the growing season at the temperate site, the Harvard Forest. We call the overall correction using PEARL the MS-PEARL correction.

3. Results and Discussion

3.1. Eddy flux carbon balance from u_* filters

We applied CPD to the binned NCE_{obs} vs. u_* relationship of all three sites to assess the carbon balance resulting from a conventional u_* filtering approach (Fig. 1). Results for u_*^{Th} detected by CPD are in Table 1. For both the Harvard Forest (growing season only) and Guyaflux sites, u_*^{Th} from CPD agreed with the commonly used literature values within the 95% confidence intervals (Urbanski et al., 2007; Bonal et al., 2008). At TNF km67, CPD found u_*^{Th} = 0.38 m s^{-1}, which is significantly greater than the commonly used literature value of u_*^{Th} = 0.22 m s^{-1} (Saleska et al., 2003; Hutyra et al., 2007; Hutyra et al. 2008). The full 7.5 year record of NCE does not demonstrate a plateau at u_* =0.22 (Fig. 1). CPD u_*^{Th} was not consistent with the literature u_*^{Th}, but was consistent with published findings that NCE still demonstrated turbulence dependence well above u_* =0.22 m s^{-1} (Saleska et al., 2003; Hutyra et al., 2007). The literature u_*^{Th} was determined by using a four-month to one-year long subset of the NCE and u_* data

(Saleska et al., 2003; Hutyra et al., 2008). Using CPD u_*^{Th} to filter NCE left only 7% of NCE available for estimating nighttime respiration. There were no unfiltered nighttime hours remaining in some months. At the Harvard Forest, CPD could not detect a u_* threshold for wintertime data (Fig. S1); we therefore applied the summertime filter to the entire eddy flux time series at this site.

The mean R at TNF km67 resulting from the CPD u_*^{Th} filter was 10.06 $\mu mol \cdot m^{-2} \cdot s^{-1}$, which resulted in a strong net source of 4.42 MgC ha^{-1} y^{-1}. Both Guyaflux and the Harvard Forest were significant sinks after applying the CPD u_*^{Th} filter, consistent with previously reported u_* filtered results (Table 1). Mean R at Guyaflux resulting from the CPD u_*^{Th} filter was 8.13 $\mu mol \cdot m^{-2} \cdot s^{-1}$, which resulted in a large net sink of 3.49 MgC ha^{-1} y^{-1} (Table 1).

All three sites had a resulting carbon balance ($NEP_{obs} = -NEE_{obs}$) that was significantly different from the mean AGWI (Table 1). Furthermore, the net carbon source at TNF km67 resulting from the CPD u_*^{Th} filter is unsustainably high; based on biomass carbon stocks estimates from Malhi et al. (2009), such emissions would result in no remaining forest biomass after 62 years. The forest was not anomalously stressed during the decade of measurements: the interannual variability in precipitation and temperature was well within the multi-decadal historical interannual variability (Hayek, 2017), making such a strong source of CO_2 unlikely at TNF km67. Similarly, at Guyaflux, the strength of the net carbon sink was unsustainable, resulting from the CPD u_*^{Th} filter would result in a doubling of forest biomass over 81 years.

The TNF km67 site showed the greatest sensitivity amongst the three sites to the choice of u_*^{Th}: the range of gap-filled NEE_{obs} corresponding to $0 \leq u_*^{Th} \leq 0.4$ m s^{-1} was 8.1 MgC ha^{-1} y^{-1} at km67 (Fig. 2), 1.5 MgC ha^{-1} y^{-1} at Guyaflux, and 1.3 MgC ha^{-1} y^{-1} at the Harvard Forest (Fig.

S2). The km67 carbon balance ranged from a significant sink to a source, while the carbon balance at Guyaflux was a significant sink regardless of the u_* filter.

Filtering data by using a different proxy for nighttime turbulence did not improve the carbon balance estimate. The recommendation by Acevedo et al. (2009) to use the standard deviation of vertical velocity fluctuations (σ_w) instead of u_* resulted in an even higher plateau of NCE at TNF km67 (10.63 $\mu mol \cdot m^{-2} \cdot s^{-1}$), hence a stronger net CO_2 source. The u_* filtered Guyaflux NEE was a strong sink of carbon, despite the AGWI over a similar time period being insignificantly different from zero (Table 1) and additional carbon reservoirs in this forest also showing little to no net accumulation of carbon (Rowland et al., 2014). We conclude that u_* filters potentially bias NEE, and may lead to unreasonable hourly and seasonal nighttime R rates and unsustainable long term net carbon budgets at the tropical forest sites.

3.2 Missing Storage Model

We optimized the parameters of the MS model according to Eqs. 3 and 4. Results for the optimized MS parameters are in Table 2. The behavior of the MS pool, C_2, over time is demonstrated for 5 days in the 2005 wet season at TNF km67 as an example case in Fig. 3. The resulting modeled storage pool C_2 tends to accumulate CO_2 at night when u_* is low, and flushes in the morning as u_* increases, until reaching the zero constraint. The time series demonstrates variability in the accumulation and flushing of the C_2 pool across different nights as u_* varies.

At each site, a single MS parameter optimization solution was found for the minimum deviation in hourly NCE_{obs} + MS from its mean value (Fig. 4; Table 2). The modeled MS flux has two regimes: accumulation ($\alpha u_* < R_2$) and flushing ($\alpha u_* > R_2$). In the accumulation regime, the MS flux is positive and decreases linearly with increasing u_*. This always corresponds to the

first condition in Eq. 3. In the flushing regime, the opposite is true: the output exceeds the input. One of two extreme scenarios typically occurs during flushing regime hours. (1) If C_2 was large enough in the previous hour to support flushing, the MS flux is negative and lands on the same MS vs. u_* line as the accumulation regime. This also corresponds to the first condition of Eq. 3. (2) If C_2 in the previous hour was zero or lower than the net flushing, then C_2 hits the boundary condition of complete mixing, because any input is immediately flushed out within that hour. This scenario corresponds to the second condition in Eq. 3, leading to weakly negative or zero net MS flux.

The resulting binned MS-corrected NCE at all three sites is presented in Fig. 5. The MS model offers an alternative explanation of the u_* change point tendency in NCE_{obs} (Fig. 1). Guyaflux and Harvard Forest have higher flushing rates α and higher mean u_* than TNF km67, and therefore attain the zero-boundary flushing scenario more frequently (Table 2), resulting in lower-NCE_{obs} plateaus and fewer pronounced negative flushing rates (Figure 4, light grey triangles). The MS model can therefore account for changes in the shape of the NCE_{obs} vs. u_* relationship between sites.

The MS flux diel pattern is synchronous and correlated with that of the measured storage flux (Fig. 6). Like the measured storage, MS is a zero-mean process over an average diurnal cycle. NEE_{obs} + MS shows both higher nighttime emission and higher daytime uptake than the original NEE. Thus, the gap-filled NEE_{obs}+MS has the same mean annual total as gap-filled NEE_{obs} without any u_* filter.

At all three sites, the first hour of nighttime NEE_{obs}+MS exhibits the highest positive flux (Fig. 6). This early nighttime "bump" was also detected in NEE_{obs} by van Gorsel et al. (2008) at a eucalyptus forest site and was used to infer the nighttime advective loss.

To elucidate the physical location of the MS pool, for which we presented some hypotheses in Section 2.3, additional analyses of preexisting measurements and novel measurement campaigns in the subcanopy airspace are needed. As an example, novel profile column measurements, located in the eddy flux footprint but without the gap associated with an eddy covariance tower, could be used to test hypothesis 1. Additionally, to test hypothesis 2, data from short subcanopy profile towers near the forest floor collected at TNF km67 and Harvard Forest as part of the respective DRAINO campaigns (Staebler and Fitzjarrald, 2004; Tóta et al., 2008), may be used to test whether near-ground accumulation is greater than that in lowest standard profile measurement (<0.5-1.0 m). Lastly, if the MS pool is instead located within the leaf litter and soil pore space (hypotheses 3), then the MS parameter R_2, our box model input rate, may be approximately equivalent to R_{soil}. Indeed, R_{soil} is approximately 4 umol $m^{-2}s^{-1}$, similar to R_2, at TNF km67 and at Harvard Forest during the summer (Hutyra et al., 2008; Giasson et al., 2017). However, estimates of R_{soil} may also be affected by turbulence and wind biases due to pressure differentials at chamber vents (Gu et al., 2002; Bain et al., 2005), imparting R_{soil} with the similar biases to those of NCE_{obs}. Additional modeling of this process may therefore be needed. Testing the various physical hypotheses is further complicated by the fact that the MS pool may have more than one physical location.

A foundational assumption of our MS model is that all unmeasured storage can be treated as a single pool on average, with one accumulation and one flushing rate. This assumption is likely violated at tropical sites with far more heterogeneous and complex terrain directly adjacent to the tower (Tóta et al., 2012) and at the Harvard Forest in the dormant season, providing qualitatively different correlations between NCE_{obs} and u_* (Fig. S1). Harvard Forest winter NCE_{obs} did not exhibit a high-u_* plateau. In contrast to winter NCE_{obs}, winter daytime NEE_{obs}

increased more rapidly with u_* as u_* increased. Differences between the summer and winter NCE_{obs} vs. u_* curves are likely related to the winter absence of a forest canopy, which has a peak summer leaf area index of 5 (Urbanksi et al., 2007). We excluded Harvard Forest dormant season from our analysis because three factors would require a more sophisticated MS model: (1) during the dormant season, leaf loss causes profile measurement-sensed airspace to ventilate easily; (2) leaf shedding adds a thick leaf litter layer seal to the forest floor, beneath which storage measurements are not present; (3) snowfall adds an additional barrier in the winter. Nonetheless, our MS model accounted for and corrected the slope-plateau behavior of NCE_{obs} at times of the year when the forest canopy was foliated at all sites.

3.3. The PEARL advection correction.

3.3.1. PEARL estimates of advective loss.

We estimated A_{night} (Eq. 5) using the PEARL approach (Eq. 6–7), illustrated for TNF km67 in Fig. 7. We compared PEARL A_{night} with that from DRAINO experiments under the assumption that these advection measurements are a reliable indication of the mean A_{night} for the entire time series. We found that PEARL agreed with measurements from both DRAINO sites within literature-reported DRAINO mean standard errors and PEARL 95% mean confidence intervals (Table 3).

We note that advective losses in physical systems may not correspond precisely to the assumption of zero u_* dependency in A_{night}. For example, Tota et al. (2008; Fig. 13 therein) still demonstrate a negative dependency of advective loss upon u_*. The effect size of this dependency is weaker than that in NEE_{obs} (Fig. 1). Through a portion of the u_* range, u_*=0.15 to u_*=0.35 m/s, there was no association or even a slight positive association with u_* instead of the presupposed

442 negative association. We inspected the TNF km67 data and found that this u_* range actually
443 represents a majority of nighttime hours, about 55%, because turbulence infrequently reaches
444 values of 0.4 m/s or greater at this site (Fig. 1). An association between A_{night} and u_* is therefore
445 not mutually exclusive with MS accounting for the majority of the variation in NEE_{obs} with
446 respect to u_* (Fig. 5).

447 More challenging, however, is that Aubinet et al. (2010) show a number of biases
448 associated with DRAINO-like measurements of horizontal and vertical advection, including
449 varying directions of u_* dependency, over- or under-compensation of a realistic nighttime flux
450 magnitude, and varying correction magnitudes from different wind sectors. We note, however,
451 that these campaigns lacked the exploratory observations that were performed in DRAIO
452 campaigns to determine optimal site-specific physical network configuration. Additionally, the
453 DRAINO campaigns sought to link the subcanopy flow processes to physical forcing, ensuring
454 that transport processes were systematic. The lack of site-specific exploratory observations,
455 performing measurement network design testing, and linking advective flows to physical
456 conditions may have played a role in not allowing Aubinet et al. (2010) to determine consistent
457 advective losses across forest sites with vastly different physical structure and terrain. The
458 DRAINO advective loss estimates were persistent across multiple years of measurement and of
459 significant importance. We therefore believe the DRAINO results represent robust estimates of
460 advective loss with which to compare our empirical PEARL estimates.

461 Uncertainties in PEARL A_{night} arise from the choice of the nonlinear functional form and
462 of the upper PAR bound for the regression. At TNF km67, various choices of upper PAR
463 threshold (from 300 to 2000 $\mu mol \cdot m^{-2} \cdot s^{-1}$), and various functional forms for NEE_{obs}+MS vs. PAR
464 (logarithmic, hyperbolic, and quadratic), resulted in a range of approximately ± 0.15 $\mu mol \cdot m^{-2} \cdot s^{-1}$

in A_{night}, which is similar to our estimated random error. We opted for a less extreme upper threshold of PAR=1000 μmol·m^{-2}·s^{-1} because the resulting PEARL A_{night} estimate was less sensitive to the choice of regression function when very high-PAR curvature was excluded. Because our lower PAR threshold of zero allowed us to evaluate the PAR-curve intercept with plenty of data near the nighttime limit, our PEARL estimates of A_{night} were robust.

A potential systematic bias in PEARL A_{night} might arise from diurnal hysteresis in R_{soil}, which is greater earlier in the night than later, even after accounting for temperature variation. However, the diurnal hysteresis in R_{soil} could be due to physical time delays, associated with molecular and thermal diffusion, and not biological ones (Phillips et al. 2011). If this hypothesis is correct, then the hysteresis in R_{soil} is likely already subsumed by MS, which accounts for diurnal hysteresis in efflux of total R (Fig. 6) via minimizing the nighttime variance NCE_{obs}+MS (Eq. 4). Alternatively, supposing that the hysteresis in R_{soil} is biological, Phillips et al. (2010) quantified the magnitude of this hysteresis for Harvard Forest. They found that, while the diel hysteresis in R_{soil} can be large (up to multiple μmol·m^{-2}·s^{-1}), the magnitude of the difference over the course of the night is on the order of 0.3 μmol·m^{-2}·s^{-1}, well below our Harvard Forest PEARL estimate of A_{night} of 1.69 μmol·m^{-2}·s^{-1} (Fig. S3). We also ruled out additional biases in PEARL A_{night} such as the Kok effect of diminishing daytime plant respiration because these effects vanish at our minimum PAR threshold of zero (Bruhn et al., 2011; Heskel et al., 2013). Consistent with the findings of van Gorsel et al., (2008), we conclude that nighttime changes in R_{soil} are likely small relative to our estimates of A_{night}.

3.3.2. Total MS-PEARL eddy flux carbon balance correction.

We inserted our PEARL A_{night} into our total correction for NEE (Eq. 2). The mean annual NEE_{obs}+MS-PEARL for all three sites are presented in Fig. 8, integrated annually and averaged for all years in the time series, presented in units of MgC ha^{-1} yr^{-1}. At both tropical sites, NEE_{obs}+MS-PEARL was within the 95% confidence intervals of the mean annual AGWI from forest biometry. The uncorrected NEE_{obs} and CPD u_*-filtered NEE_{obs} were significantly different from AGWI (Fig 8; Table 3). At Harvard Forest, the MS-PEARL correction moved NEE only partially closer to AGWI, but the correction was only applied to the growing season.

The sign of the Guyaflux AGWI and NEE_{obs}+MS-PEARL are opposite, although most of the net AGWI loss stemmed from a single large mortality event in 2006, associated with windfall from storms during the wet season. Because these fallen trees can take multiple decades to decompose (Hérault et al., 2010), a lag in their contribution to NEE would only be apparent over longer integration times. An additional set of surveys at the Paracou site surrounding Guyaflux, spanning 16 years (1991-2007) in adjacent intact forest plots, found net AGWI accrual of 0.45 MgC ha^{-1} y^{-1}, primarily in the largest trees (Rutishauser et al., 2010).

Our comparison between MS-PEARL corrected NEE and AGWI is limited because AGWI only quantifies net carbon accumulation or loss in live aboveground woody biomass (including only trees greater than 10 cm diameter), whereas NEE quantifies net carbon accumulation or loss in all ecosystem pools (NEE = -NEP = -NPP + heterotrophic R = -GPP + autotrophic R + heterotrophic R), including other live aboveground biomass (e.g. small trees), live belowground biomass (e.g. roots), and dead biomass (e.g. decaying wood, plant matter and soil).

Complete surveys of fluxes from all carbon pools have accounted comprehensively for NPP, heterotrophic R, and their difference, NEE, at both tropical sites (Malhi et al., 2009;

510 Rowland et al., 2014). NEE totaled 0.5 and -0.3 MgC $ha^{-1}yr^{-1}$ for TNF km67 and Guyaflux
511 respectively. Fluxes from individual carbon pools were measured at year-long or longer
512 intervals, but were non-simultaneous, spanned less than a decade, and had large errors from
513 limited sampling of pools, which compounded to more than 3 MgC ha^{-1} y^{-1} in aggregate.
514 However, of the individual live and dead carbon pools, these pools only lost or accrued biomass
515 at a rate of less than 15% of AGWI on an annual basis, with exception to CWD at km67 (0.8±0.9
516 MgC ha^{-1} yr^{-1} annual net loss in 2001-2005) (Rice et al., 2004; Hutyra et al., 2008; Malhi et al.,
517 2009). More recent surveys of the TNF km67 CWD pool, however, indicate that this pool too
518 has equilibrated (Hayek, 2017), with inputs to and losses from this pool being approximately
519 equivalent after 2005 (0.02±0.6 MgC ha^{-1} yr^{-1} annual net accrual). An updated whole-forest NEE
520 result for TNF km67 using the equilibrated CWD flux and Malhi et al. (2009) net fluxes for other
521 carbon stocks would therefore be -0.3 MgC ha^{-1} yr^{-1} (net accrual). Although extensive,
522 simultaneous, and frequent bottom-up inventories of NEE, including all relevant autotrophic and
523 heterotrophic *R* fluxes, are challenging, they are a necessary future step to reduce errors and
524 definitively validate the MS-PEARL correction. Nonetheless, the accrual or losses in pools other
525 than AGWB were in aggregate less than the 95% confidence intervals for random measurement
526 errors in our estimates of AGWI. AGWI therefore provides a reasonable means for
527 approximating whole-forest NEE in the case of these two forests. Forest inventories, whether
528 examining the long-term AGWI or shorter-term annual whole-forest NEE, agree with MS-
529 PEARL results that the two tropical forests are in fact slight sinks, closer to carbon-neutral than
530 the CPD u_*-filter results (Table 3) suggest.
531 Results for MS-PEARL-corrected mean nighttime *R* at the TNF km67 site were
532 consistent with previous literature estimates that applied $u_*^{Th} = 0.22$ to the first four years of eddy

flux data (Hutyra et al., 2007). An independent flux estimate using continuous measurements of Radon-222 (^{222}Rn) as a tracer of CO_2 exchange (Martens et al., 2004) quantified one full year of R as 7.9 ± 0.8 μmol·m^{-2}·s^{-1}, which agreed with literature R (u_*^{Th}=0.22) = 8.6 ± 0.1 μmol·m^{-2}·s^{-1} (Hutyra et al., 2008) and with our MS-PEARL correction R = 8.79 ± 0.26 μmol·m^{-2}·s^{-1}. An additional three years of eddy flux data, however, resulted in a divergence between NEE_{obs} (u_*^{Th}=0.22) and NEE_{obs}+MS-PEARL that differs in sign and magnitude (Fig. 8). Our findings therefore do not contradict previous independently verified estimates of the nighttime carbon budget. Rather, as additional eddy covariance data have become available, our results suggest that the u_* filter paradigm for correction of flux biases has become increasingly in need of replacement.

Provided that our underlying assumptions are correct, the MS-PEARL framework presents a reliable means of correcting selective systematic biases in multi-year NEE records, but it should be used cautiously in analyses (e.g. model-data fusion approaches) at the native hourly resolution of eddy flux measurements. One reason is that empirical parameter fitting in our approach (e.g. Eq. 3-4) makes MS-corrected measurements more contaminated by empirically modeled output, even more so when combined with typical gap-filling approaches using PAR and temperature regression model outputs (Falge et al., 2001; Dunn et al., 2007; Urbanksi et al., 2007). Additionally, estimating advective loss relies on multi-year sets of hourly data used in model fitting (Eq. 6). The resulting A_{night} is a constant offset, providing no information about the inter-hour variability of the advective divergence loss process relative to NEE_{obs}.

Small error bounds for the PEARL A_{night} estimate depend on very long time series of eddy flux data. For the 10-year record at Paracou, 95% confidence intervals were ±0.4 MgC ha^{-1} y^{-1}. Evaluating this quantity for only the year 2013 increased the error to ±1.3 MgC ha^{-1}·y^{-1} due

to the smaller sample size. The findings of this study therefore highlight the need for long-term decadal eddy covariance measurement campaigns reduce uncertainties in the net terrestrial carbon balance.

5. Conclusions

Although the u_* filter has remained the preferred approach to addressing biases in eddy covariance measurements for more than twenty years, results from two tropical forest sites demonstrate that this correction can result in biased hourly nighttime respiration rates and large uncertainty in the long-term ecosystem carbon balance, including sums that are physically unrealistic. The data retention rate can also be very low—as little as 7% at one tropical site. We considered MS as an alternative simple model to the u_* filter to explain turbulence biases in NCE_{obs}. The MS model accounted for slope-plateau behavior of the NCE_{obs} vs. u_* relationship and provided a sensible explanation for the variation in curve shape between sites, without discarding any data.

After correcting NEE_{obs} by MS, we have demonstrated that PEARL nocturnal advective divergence loss estimates show good agreement with DRAINO measurements and produce reasonable estimates of long-term carbon balance. PEARL may therefore be an especially effective method for estimating advective divergence loss at sites where direct measurements are not available.

Future investigations are needed into the speculative hypotheses underlying the MS-PEARL and u_* filter approaches, in order to determine which method has more physically sound hypotheses. Additional work is needed to account for the effects of leaf shedding and snowfall

upon MS in the temperate forest dormant season, when both the u_* filter and MS-PEARL approaches fail. Contingent upon the results of such investigations, the MS-PEARL correction has potential for widespread application to eddy covariance estimates of the long-term carbon balance in global forests.

Acknowledgements

This work was supported by funding from a National Science Foundation PIRE fellowship (OISE 0730305) and a U.S. Department of Energy grant (DE-SC0008311). The km67 eddy flux data used in this study are available online via the Oak Ridge National Laboratory (ORNL) Ameriflux network database at ftp://cdiac.ornl.gov/pub/ameriflux/data/Level2/Sites_ByID/BR-Sa1. Further site description and data links are available online at ORNL Fluxnet http://fluxnet.ornl.gov/site/83.

We thank Benoit Burban who technically manages the Guyaflux site. The Guyaflux program belongs to the SOERE F-ORE-T which is supported annually by Ecofor, Allenvi and the French national research infrastructure ANAEE-F. The Guyaflux program also received support from the "Observatoire du Carbone en Guyane" and an "investissement d'avenir" grant from the Agence Nationale de la Recherche (CEBA, ref ANR-10-LABX-25-01).

Citations

Acevedo, O., Moraes, O., Degrazia, G., Fitzjarrald, D., Manzi, a, Campos, J., 2009. Is friction velocity the most appropriate scale for correcting nocturnal carbon dioxide fluxes? Agric. For. Meteorol. 149, 1–10. doi:10.1016/j.agrformet.2008.06.014

Aubinet, M., Heinesch, B., Yernaux, M., 2003. Horizontal and vertical CO2 advection in a sloping forest. Boundary-Layer Meteorol. 108, 397–417. doi:10.1023/A:1024168428135

Aubinet, M., Feigenwinter, C., Heinesch, B., Bernhofer, C., Canepa, E., Lindroth, A., Montagnani, L., Rebmann, C., Sedlak, P., Van Gorsel, E., 2010. Direct advection measurements do not help to solve the night-time CO2 closure problem: Evidence from three different forests. Agric. For. Meteorol. 150, 655–664. doi:10.1016/j.agrformet.2010.01.016

608 Bain, W.G., Hutyra, L., Patterson, D.C., Bright, A. V., Daube, B.C., Munger, J.W., Wofsy, S.C., 2005. Wind-
609 induced error in the measurement of soil respiration using closed dynamic chambers. Agric. For. Meteorol.
610 131, 225–232. doi:10.1016/j.agrformet.2005.06.004

611 Barr, A.G., Richardson, A.D., Hollinger, D.Y., Papale, D., Arain, M. a., Black, T. a., Bohrer, G., Dragoni, D.,
612 Fischer, M.L., Gu, L., Law, B.E., Margolis, H. a., McCaughey, J.H., Munger, J.W., Oechel, W., Schaeffer, K.,
613 2013. Use of change-point detection for friction–velocity threshold evaluation in eddy-covariance studies.
614 Agric. For. Meteorol. 171–172, 31–45. doi:10.1016/j.agrformet.2012.11.023

615 Bonal, D., Bosc, A., Ponton, S., Goret, J.-Y., Burban, B., Gross, P., Bonnefond, J.-M., Elbers, J., Longdoz, B.,
616 Epron, D., Guehl, J.-M., Granier, A., 2008. Impact of severe dry season on net ecosystem exchange in the
617 Neotropical rainforest of French Guiana. Glob. Chang. Biol. 14, 1917–1933. doi:10.1111/j.1365-
618 2486.2008.01610.x

619 Bruhn, D., Mikkelsen, T.N., Herbst, M., Kutsch, W.L., Ball, M.C., Pilegaard, K., 2011. Estimating daytime
620 ecosystem respiration from eddy-flux data. BioSystems 103, 309–313. doi:10.1016/j.biosystems.2010.10.007

621 Dunn, A.L., Barford, C.C., Wofsy, S.C., Goulden, M.L., Daube, B.C., 2007. A long-term record of carbon exchange
622 in a boreal black spruce forest: means, responses to interannual variability, and decadal trends. Glob. Chang.
623 Biol. 13, 577–590. doi:10.1111/j.1365-2486.2006.01221.x

624 Falge, E., Baldocchi, D., Olson, R., Anthoni, P., Aubinet, M., Bernhofer, C., Burba, G., Ceulemans, R., Clement, R.,
625 Dolman, H., Granier, A., Gross, P., Grünwald, T., Hollinger, D., Jensen, N.-O., Katul, G., Keronen, P.,
626 Kowalski, A., Lai, C.T., Law, B.E., Meyers, T., Moncrieff, J., Moors, E., Munger, J.W., Pilegaard, K., Rannik,
627 Ü., Rebmann, C., Suyker, A., Tenhunen, J., Tu, K., Verma, S., Vesala, T., Wilson, K., Wofsy, S., 2001. Gap
628 filling strategies for defensible annual sums of net ecosystem exchange. Agric. For. Meteorol. 107, 43–69.
629 doi:10.1016/S0168-1923(00)00225-2

630 Galvagno, M., Wohlfahrt, G., Cremonese, E., Filippa, G., Migliavacca, M., Mora, U., Cella, D., Van Gorsel, E.,
631 2017. Contribution of advection to nighttime ecosystem respiration at a mountain grassland in complex
632 terrain. Agric. For. Meteorol. 237–238, 270–281. doi:10.1016/j.agrformet.2017.02.018

633 Goulden, M.L., Munger, J.W., Fan, S.-M., Daube, B.C., Wofsy, S.C., 1996. Measurements of carbon sequestration
634 by long-term eddy covariance: Methods and a critical evaluation of accuracy. Glob. Chang. Biol. [Global
635 Chang. Biol.] 2, 169–182. doi:10.1111/j.1365-2486.1996.tb00070.x

636 Hayek, M., 2017. Drivers of Long-Term Variability in Amazon Forest Carbon Fluxes. Doctoral dissertation.
637 Harvard University.

638 Hérault, B., Beauchêne, J., Muller, F., Wagner, F., Baraloto, C., Blanc, L., Martin, J.-M., 2010. Modeling decay
639 rates of dead wood in a neotropical forest. Oecologia 164, 243–51. doi:10.1007/s00442-010-1602-8

640 Heskel, M. a, Atkin, O.K., Turnbull, M.H., Griffin, K.L., 2013. Bringing the Kok effect to light: A review on the
641 integration of daytime respiration and net ecosystem exchange. Ecosphere 4, 1–14. doi:10.1890/Es13-00120.1

642 Hutyra, L.R., Munger, J.W., Saleska, S.R., Gottlieb, E., Daube, B.C., Dunn, A.L., Amaral, D.F., de Camargo, P.B.,
643 Wofsy, S.C., 2007. Seasonal controls on the exchange of carbon and water in an Amazonian rain forest. J.
644 Geophys. Res. Biogeosciences 112, G03008. doi:10.1029/2006JG000365

645 Hutyra, L.R., Munger, J.W., Hammond-Pyle, E., Saleska, S.R., Restrepo-Coupe, N., Daube, B.C., de Camargo, P.B.,
646 Wofsy, S.C., 2008. Resolving systematic errors in estimates of net ecosystem exchange of CO2 and ecosystem
647 respiration in a tropical forest biome. Agric. For. Meteorol. 148, 1266–1279.
648 doi:10.1016/j.agrformet.2008.03.007

649 IPCC: Summary for policymakers, in: Climate change 2013: the physical science basis. Contribution of working
650 group I to the fifth assessment report of the Intergovernmental Panel on Climate Change, 2013. Edited by
651 Stocker, T. F., Qin, D., Plattner, G.-K., Tignor, M., Allen, S. K., Boschung, J., Nauels, A., Xia, Y., Bex, V.,
652 and Midgley, P. M.. pp. 1–33. Cambridge Univ. Press, Cambridge, UK and New York, NY, USA.

Lee, X., 1998. On micrometeorological observations of surface-air exchange over tall vegetation. Agric. For. Meteorol. 91, 39–49. doi:10.1016/S0168-1923(98)00071-9

Malhi, Y., Saatchi, S., Girardin, C., Aragão, L.E.O.C., 2009. The production, storage, and flow of carbon in Amazonian forests, in: Amazonia and Global Change. pp. 355–372. doi:10.1029/2008GM000779

Martens, C., Shay, T., Mendlovitz, H., Matross, D., Saleska, S., Wofsy, S., Woodward, S., Mentons, M., Moura, J., Crill, P., De Moraes, O., Lima, R., 2004. Radon uxes in tropical forest ecosystems of Brazilian Amazonia: night-time CO 2 net ecosystem exchange derived from radon and eddy covariance methods. Glob. Chang. Biol. 618–629. doi:10.1111/j.1529-8817.2003.00764.x

Miller, S.D., Goulden, M.L., Menton, M.C., Da Rocha, H.R., De Freitas, H.C., E Silva Figueira, A.M., De Sousa, C.A.D., 2004. Biometric and micrometeorological measurements of tropical forest carbon balance. Ecol. Appl. 14, 114–126. doi:10.1890/02-6005

Moncrieff, J.B., Malhi, Y., Leuning, R., Mahli, Y., Leuning, R., 1996. The propagation of errors in long-term measurements of land-atmosphere fluxes of carbon and water. Glob. Chang. Biol. 2, 231–240. doi:10.1111/j.1365-2486.1996.tb00075.x

Papale, D., Reichstein, M., Aubinet, M., Canfora, E., Bernhofer, C., Kutsch, W., Longdoz, B., Rambal, S., Valentini, R., Vesala, T., Yakir, D., 2006. Towards a standardized processing of Net Ecosystem Exchange measured with eddy covariance technique: algorithms and uncertainty estimation. Biogeosciences 3, 571–583. doi:10.5194/bg-3-571-2006

Phillips, C.L., Nickerson, N., Risk, D., Bond, B.J., 2011. Interpreting diel hysteresis between soil respiration and temperature. Glob. Chang. Biol. 17, 515–527. doi:10.1111/j.1365-2486.2010.02250.x

Phillips, S.C., Varner, R.K., Frolking, S., Munger, J.W., Bubier, J.L., Wofsy, S.C., Crill, P.M., 2010. Interannual, seasonal, and diel variation in soil respiration relative to ecosystem respiration at a wetland to upland slope at Harvard Forest. J. Geophys. Res. 115, 1–18. doi:10.1029/2008JG000858

Pyle, E.H., Santoni, G.W., Nascimento, H.E.M., Hutyra, L.R., Vieira, S., Curran, D.J., Van Haren, J., Saleska, S.R., Chow, V.Y., Carmago, P.B., Laurance, W.F., Wofsy, S.C., 2009. Dynamics of carbon, biomass, and structure in two Amazonian forests. J. Geophys. Res. Biogeosciences 114. doi:10.1029/2007JG000592

Reichstein, M., Falge, E., Baldocchi, D., Papale, D., Aubinet, M., Berbigier, P., Bernhofer, C., Buchmann, N., Gilmanov, T., Granier, A., Gr??nwald, T., Havr??nkov??, K., Ilvesniemi, H., Janous, D., Knohl, A., Laurila, T., Lohila, A., Loustau, D., Matteucci, G., Meyers, T., Miglietta, F., Ourcival, J.M., Pumpanen, J., Rambal, S., Rotenberg, E., Sanz, M., Tenhunen, J., Seufert, G., Vaccari, F., Vesala, T., Yakir, D., Valentini, R., 2005. On the separation of net ecosystem exchange into assimilation and ecosystem respiration: Review and improved algorithm. Glob. Chang. Biol. 11, 1424–1439. doi:10.1111/j.1365-2486.2005.001002.x

Rice, A.H., Pyle, E.H., Saleska, S.R., Hutyra, L., Palace, M., Keller, M., de Camargo, P.B., Portilho, K., Marques, D.F., Wofsy, S.C., 2004. Carbon Balance and Vegetation Dynamics in an Old-Growth Amazonian Forest. Ecol. Appl. 14, 55–71. doi:10.1890/02-6006

Rowland, L., Hill, T.C., Stahl, C., Siebicke, L., Burban, B., Zaragoza-Castells, J., Ponton, S., Bonal, D., Meir, P., Williams, M., 2014. Evidence for strong seasonality in the carbon storage and carbon use efficiency of an Amazonian forest. Glob. Chang. Biol. 20, 979–991. doi:10.1111/gcb.12375

Rutishauser, E., Wagner, F., Herault, B., Nicolini, E.A., Blanc, L., 2010. Contrasting above-ground biomass balance in a Neotropical rain forest. J. Veg. Sci. 21, 672–682. doi:10.1111/j.1654-1103.2010.01175.x

Saleska, S.R., Miller, S.D., Matross, D.M., Goulden, M.L., Wofsy, S.C., da Rocha, H.R., de Camargo, P.B., Crill, P., Daube, B.C., de Freitas, H.C., Hutyra, L., Keller, M., Kirchhoff, V., Menton, M., Munger, J.W., Pyle, E.H., Rice, A.H., Silva, H., 2003. Carbon in Amazon forests: unexpected seasonal fluxes and disturbance-induced losses. Science 302, 1554–7. doi:10.1126/science.1091165

697 Staebler, R.M., Fitzjarrald, D.R., 2004. Observing subcanopy CO2 advection. Agric. For. Meteorol. 122, 139–156.
698 doi:10.1016/j.agrformet.2003.09.011

699 Staebler, R.M., Fitzjarrald, D.R., 2005. Measuring Canopy Structure and the Kinematics of Subcanopy Flows in
700 Two Forests. J. Appl. Meteorol. 44, 1161–1179. doi:10.1175/JAM2265.1

701 Sun, J., Desjardins, R.L., Mahrt, L., MacPherson, J.I., 1998. Transport of carbon dioxide, water vapor, and ozone by
702 turbulence and local circulations. J. Geophys. Res. 103, 25873–25885. doi:10.1029/98JD02439

703 Tóta, J., Fitzjarrald, D.R., Staebler, R.M., Sakai, R.K., Moraes, O.M.M., Acevedo, O.C., Wofsy, S.C., Manzi, A.O.,
704 2008. Amazon rain forest subcanopy flow and the carbon budget: Santarém LBA-ECO site. J. Geophys. Res.
705 Biogeosciences 113, n/a-n/a. doi:10.1029/2007JG000597

706 Tóta, J., Roy Fitzjarrald, D., da Silva Dias, M.A.F., 2012. Amazon Rainforest Exchange of Carbon and Subcanopy
707 Air Flow: Manaus LBA Site—A Complex Terrain Condition. Sci. World J. 2012, 1–19.
708 doi:10.1100/2012/165067

709 Urbanski, S., Barford, C., Wofsy, S., Kucharik, C., Pyle, E., Budney, J., McKain, K., Fitzjarrald, D., Czikowsky, M.,
710 Munger, J.W., 2007. Factors controlling CO2 exchange on timescales from hourly to decadal at Harvard
711 Forest. J. Geophys. Res. Biogeosciences 112, G02020. doi:10.1029/2006JG000293

712 van Gorsel, E., Leuning, R., Cleugh, H.A., Keith, H., Suni, T., 2007. Nocturnal carbon efflux: Reconciliation of
713 eddy covariance and chamber measurements using an alternative to the u * -threshold filtering technique.
714 Tellus, Ser. B Chem. Phys. Meteorol. 59, 397–403. doi:10.1111/j.1600-0889.2007.00252.x

715 van Gorsel, E., Leuning, R., Cleugh, H.A., Keith, H., Kirschbaum, M.U.F., Suni, T., 2008. Application of an
716 alternative method to derive reliable estimates of nighttime respiration from eddy covariance measurements in
717 moderately complex topography. Agric. For. Meteorol. 148, 1174–1180. doi:10.1016/j.agrformet.2008.01.015

718 Wofsy, S.C., Goulden, M.L., Munger, J.W., Fan, S.M., Bakwin, P.S., Daube, B.C., Bassow, S.L., Bazzaz, F. a,
719 1993. Net Exchange of CO2 in a Mid-Latitude Forest. Science (80-.). doi:10.1126/science.260.5112.1314

Site	Lit.	CPD				Mean annual AGWI (MgC ha^{-1} y^{-1})
	u_*^{Th} (m s^{-1})	u_*^{Th} (m s^{-1})	NCE data remaining	Advective loss (μmol m^{-2} s^{-1})	Mean annual NEP (MgC ha^{-1} y^{-1})	
TNF km67	0.22	0.38 (0.34, 0.40)	7%	3.95 (3.63, 4.01)	-4.42 (-5.07, -3.87)	0.39 (-1.29, 2.12)
Guyaflux	0.15	0.16 (0.15, 0.18)	60%	0.42 (0.40,0.45)	3.49 (3.29, 3.69)	-.46 (-2.12, 1.04)
Harvard Forest (summer)	0.20	0.22 (0.19, 0.26)	59%	0.73 (0.69, 0.75)	2.96 (2.88, 3.04)	1.60 (-1.43, 1.76)

Table 1. Literature and CPD u_*^{Th}, with the resulting CPD u_*^{Th} advective loss and carbon balance. NEP and AGWI have the same sign convention (NEP = -NEE): positive corresponds to net carbon accrual and negative corresponds to carbon loss. For Harvard Forest, the summer u_*^{Th} was applied to NEP for the entire year. 95% confidence intervals are in parentheses.

Site	R_2 (μmol m^{-2} s^{-1})	α (μmol m^{-3})	Mean nighttime u_* (m s^{-1}) (±SD)	Proportion of nighttime flushing hours when $dC_2/dt=0$
TNF km67	4.7	18	0.19 (±0.11)	20.8%
Guyaflux	4.2	26	0.21 (±0.14)	80.7%
Harvard Forest (summer)	4.5	22	0.31 (±0.19)	86.6%

Table 2. Parameters for MS model.

Site	Advective Loss (μmol m^{-2} s^{-1})			Mean Annual NEE (MgC ha^{-1} y^{-1})			
	CPD u_* filter	DRAINO	PEARL	NEE_{obs} no u* filter	CPD u_* filter	MS-DRAINO	MS-PEARL
TNF km67	3.95 (3.63, 4.01)	0.99	1.05 (0.83,1.27)	-3.10 (-3.24, -2.94)	4.42 (3.88, 5.08)	-0.94 (-1.10, -0.78)	-0.92 (-1.50, -0.32)
Guyaflux	0.42 (0.40,0.45)	-	1.91 (1.66, 2.18)	-4.34 (-4.51, -4.15)	-3.49 (-3.70, -3.29)	-	-0.84 (-1.39, -0.30)
Harvard Forest (summer only)	0.73 (0.69, 0.75)	1.36 (1.16, 1.56)	1.69 (1.36, 2.05)	-3.57 (-3.65, -3.50)	-2.96 (-3.04, -2.89)	-2.88 (-3.07, -2.71)	-2.72 (-2.91, -2.51)

Table 3. Mean advective loss and annual NEE before and after DRAINO and PEARL corrections for each site. 95% confidence intervals in parentheses. For Harvard Forest, the mean annual NEE was only corrected for the summer season MS-PEARL, making this an incomplete correction.

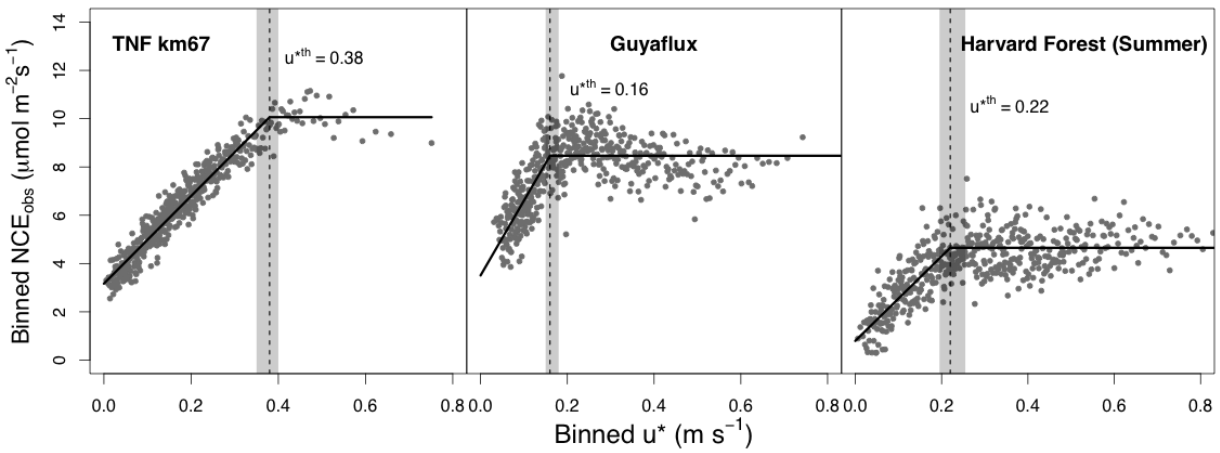

Fig. 1. Binned NCE by equally sized u_* classes (N_B = 500). Solid black line is the best-fit change-point regression from Eq. 1. Vertical dotted line is the CPD detected u*th. Shaded area is the 95% confidence interval of CPD u_*^{Th}.

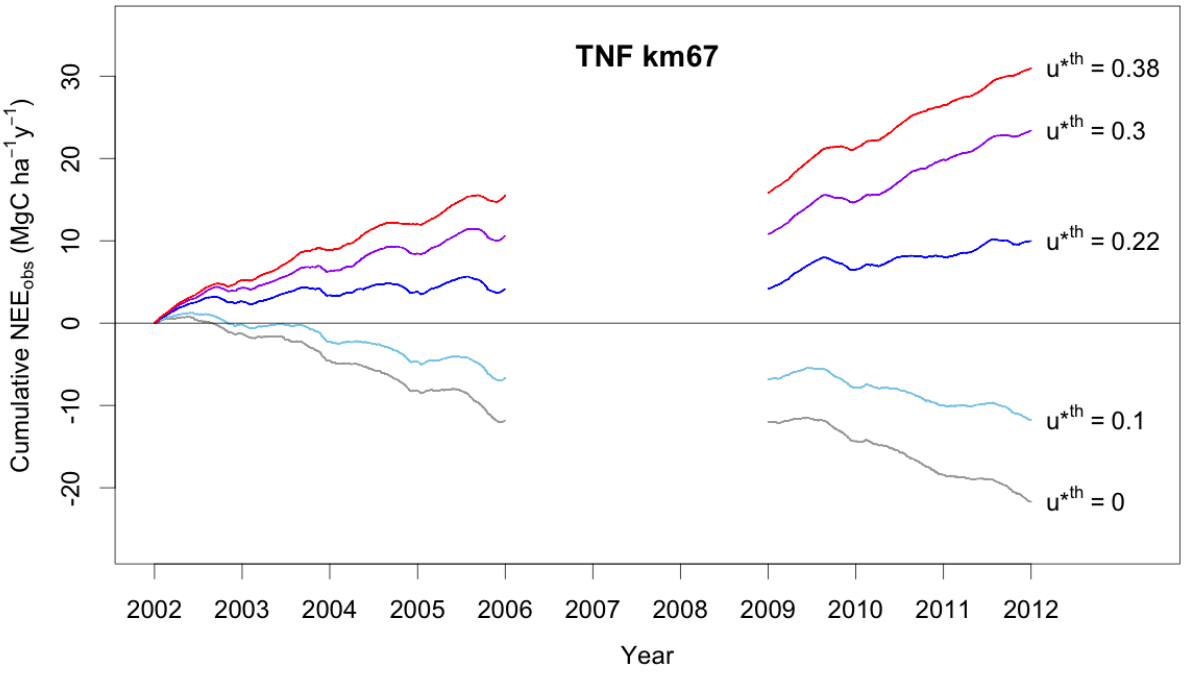

Fig. 2. TNF km67 net cumulative carbon balance from January 1, filtered by various u_*^{Th}. The cumulative sum was not reset during the 2006-2008 gap.

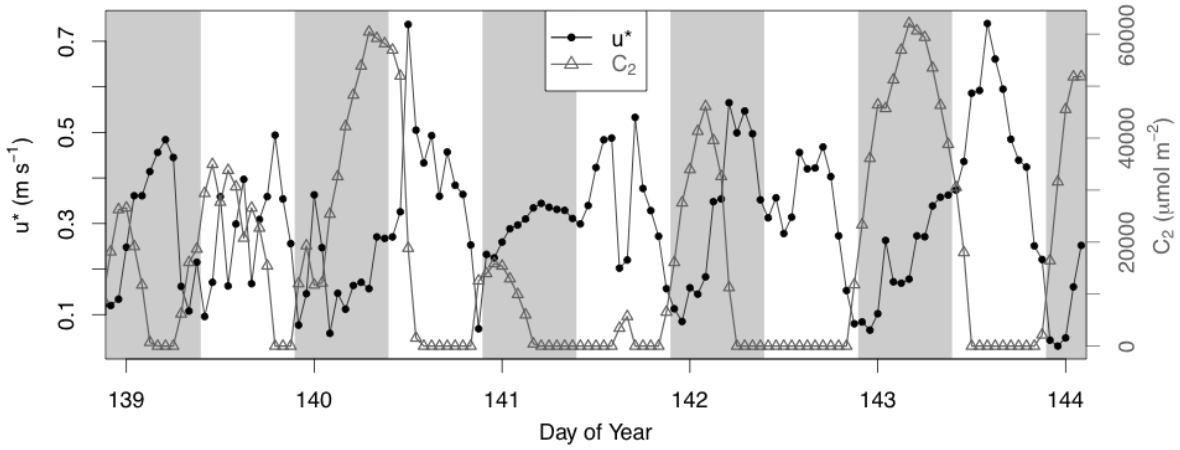

Fig. 3: Example of the hourly time series of missing storage pool concentration enhancement C_2 (grey triangles) plotted with u_* time series (black dots) for TNF km67 from May 18-24, 2005. Light grey shaded areas are nighttime hours.

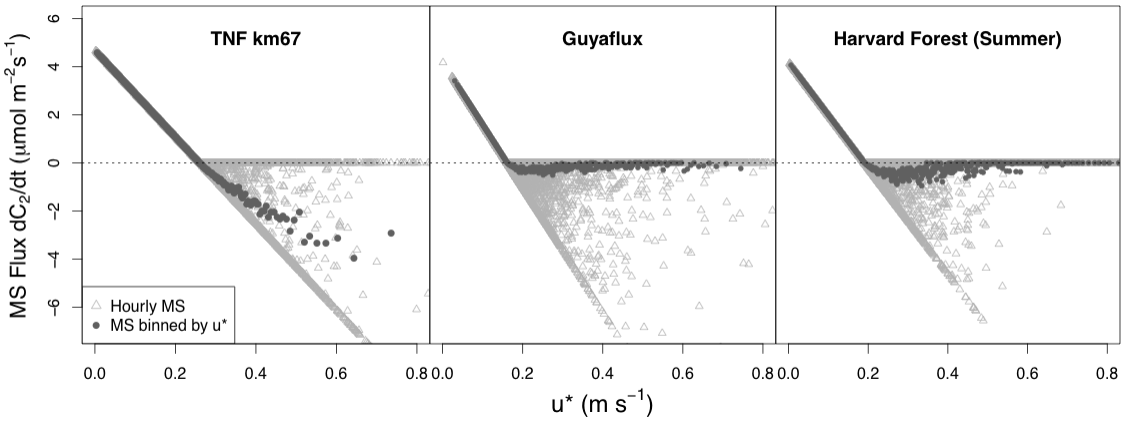

Fig. 4. Modeled MS vs u_*, hourly (light grey triangles) and binned by equally sized u_* classes, as in Figure 1 (dark grey circles). Positive values are accumulation and negative are flushing.

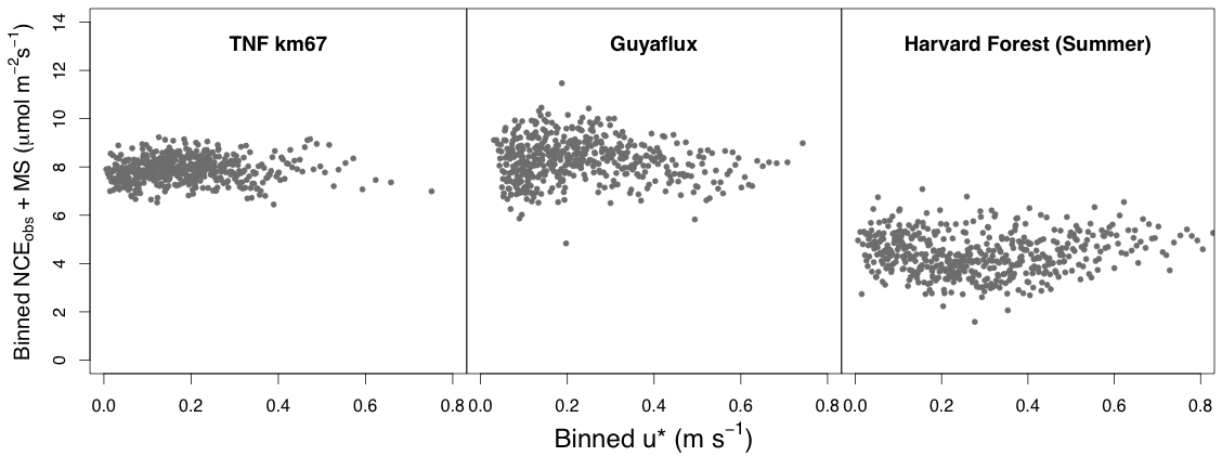

Fig. 5. Binned MS-corrected NCE vs. u_*.

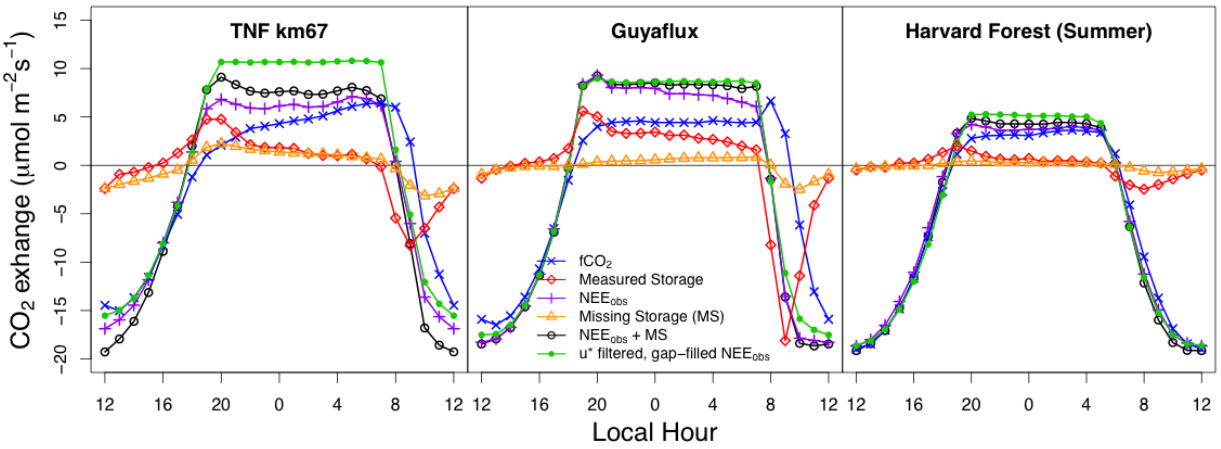

Fig. 6. Mean diurnal cycle of measured fluxes and MS correction.

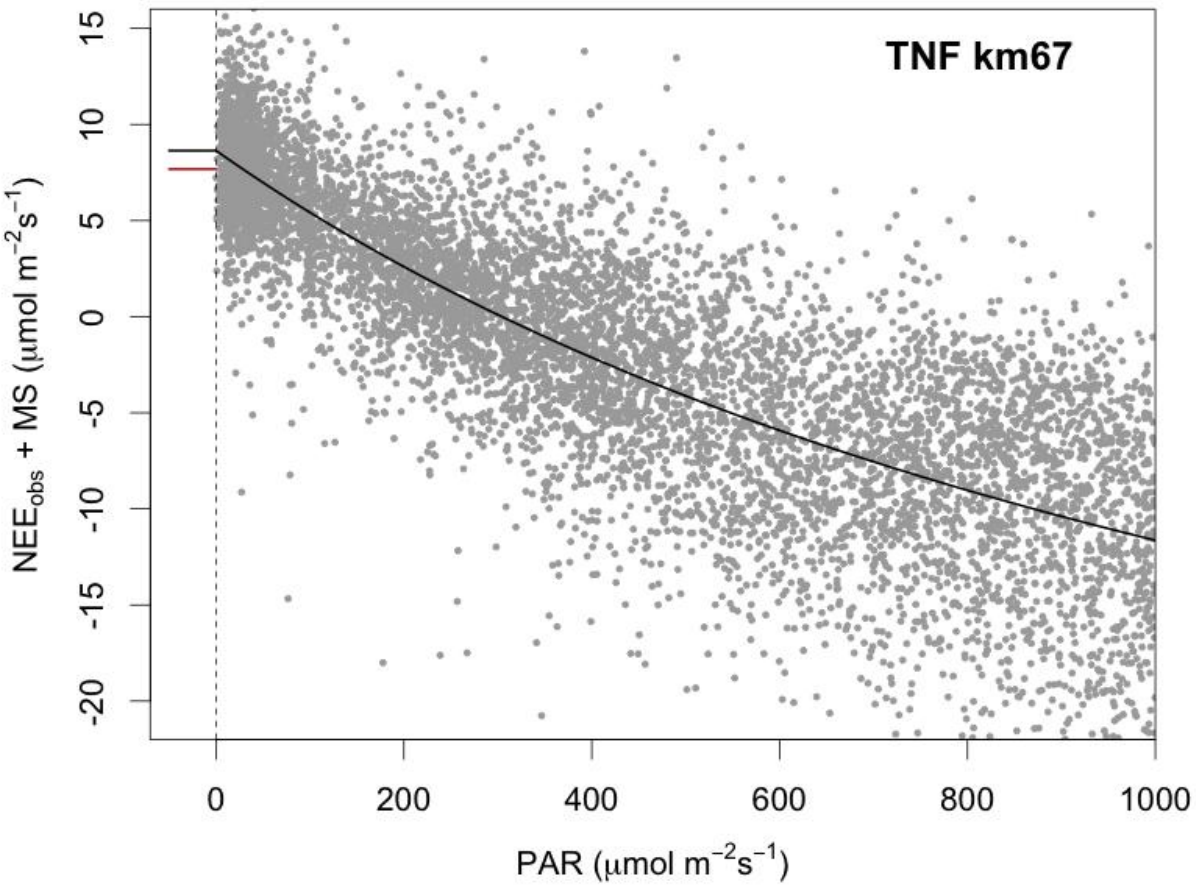

Fig. 7. Evening MS-corrected hourly NEE vs. PAR for PAR>0 (grey points) at TNF km67. Black line is the best fit nonlinear regression (Eq. 6; $a_2 = 0$). Black line segment to the left of the y-intercept is the respiration parameter a_1, the limit of evening NEE_{obs}+MS as PAR approaches zero. Red line segment is mean NCE_{obs}+MS. The difference between the two line segments is the PEARL estimate for A_{night} = 1.05 umol $m^{-2} \cdot s^{-1}$ for TNF km67.

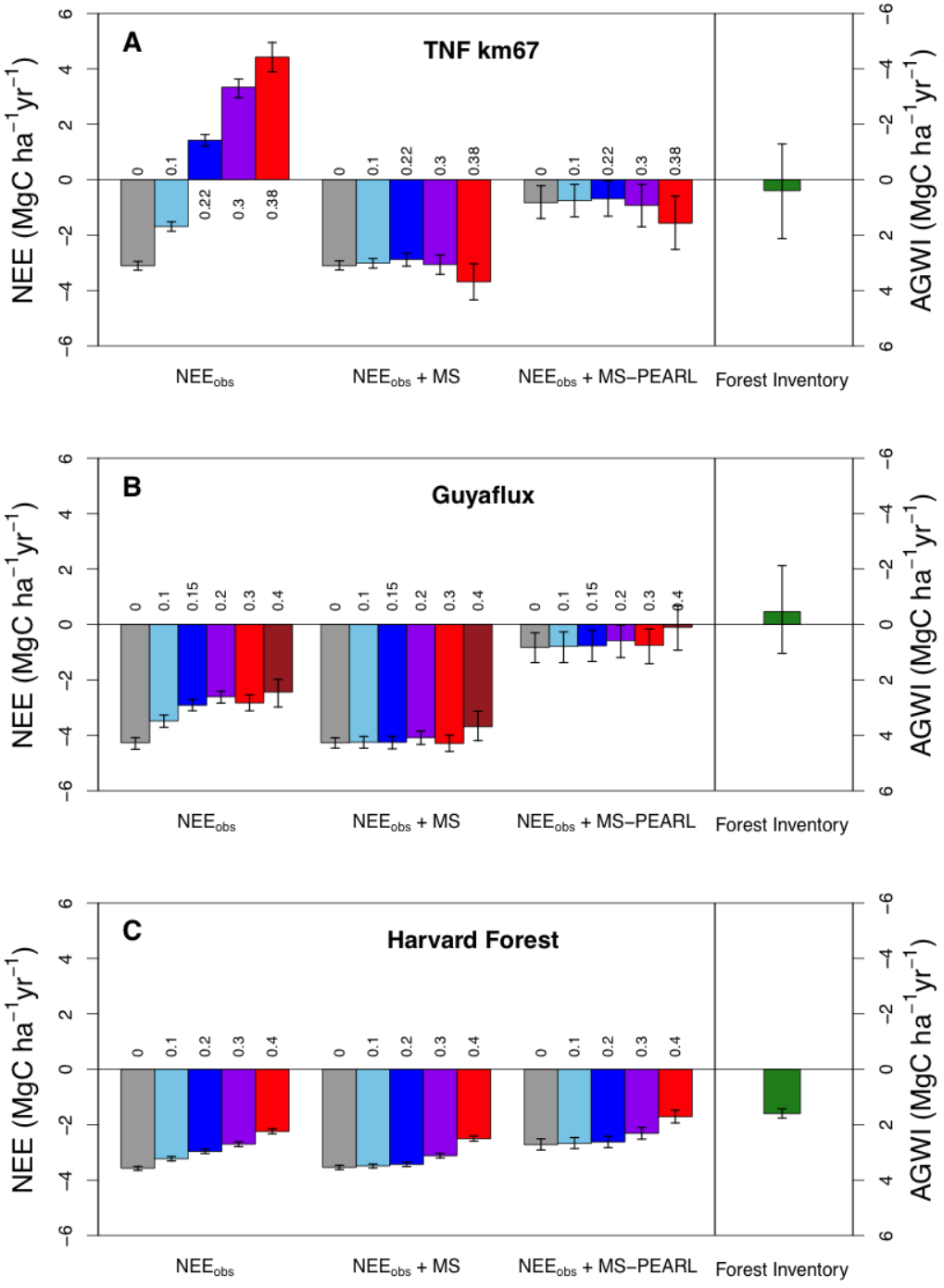

Fig. 8. Mean annually integrated NEE with respect to various u_* filters (u_*^{Th} above or below bars) for each stage of the MS-PEARL correction, compared with AGWI derived from forest inventories for (A) TNF km67 (B) Guyaflux (C) Harvard Forest. For Harvard Forest, the MS and PEARL corrections were not applied for the full year, only the growing season, because no u_*^{Th} could be found during the dormant season and so the MS correction could not be reliably implemented. Error bars represent 95% bootstrap confidence intervals, representing hourly random measurement errors on mean annual estimates.